Higher-order schemes for 3-D traveltimes and amplitudes

Songting Luo[1], **Jianliang Qian**[2] **and Hongkai Zhao**[3]

[1] *Department of Mathematics, Michigan State University, East Lansing, MI 48824. Email:* **luos@math.msu.edu**

[2] *Department of Mathematics, Michigan State University, East Lansing, MI 48824. Email:* **qian@math.msu.edu**

[3] *Department of Mathematics, University of California, Irvine, CA 92697-3875. Email:* **zhao@math.uci.edu**

(October 31, 2010)

Running head: **3-D traveltimes and amplitudes**

ABSTRACT

In the geometrical-optics approximation for the Helmholtz equation with a point source, traveltimes and amplitudes have upwind singularities at the source. Consequently, both first-order and higher-order finite-difference solvers exhibit formally at most first-order convergence and relatively large errors. Such singularities can be factored out by introducing appropriate factorizations for traveltimes and amplitudes, where one factor is a known function capturing the corresponding source singularity and the other factor is an unknown function smooth in the neighborhood of the source. The resulting underlying unknown functions satisfy factored eikonal and transport equations, respectively. A third-order weighted essentially non-oscillatory (WENO) based Lax-Friedrichs scheme is designed to compute the underlying functions. Thus highly accurate traveltimes and reliable amplitudes can be computed. Furthermore, we construct the asymptotic wave fields using computed traveltimes and amplitudes in the WKBJ form. 2-D and 3-D examples demonstrate the performance of the proposed algorithms, and the constructed WKBJ Green functions are in good agreement with direct solutions of the Helmholtz equation before caustics occur.

INTRODUCTION

In geometrical-optics approximations for high frequency wave propagation, the point-source traveltime has an upwind source singularity which makes it extremely difficult to numerically compute the traveltime field with high accuracy even by higher-order finite-difference eikonal solvers. The resultant inaccurate traveltimes prevent reliable computations of takeoff angles, out-of-plane curvatures and amplitudes. Even with accurate traveltime fields, the source singularity of takeoff angles, out-of-plane curvatures and amplitudes can also make it difficult to obtain high accuracy with usual finite-difference schemes.

Many finite-difference schemes have been introduced to solve the eikonal equation with point-source conditions (Vidale (1990); van Trier and Symes (1991); Qin et al. (1992); Schneider et al. (1992); Schneider (1995); Sethian and Popovici (1999); Kim and Cook (1999); Qian and Symes (2002a,b); Zhao (2005); Tsai et al. (2003); Qian et al. (2007b,a); Kao et al. (2005); Leung and Qian (2006); Benamou et al. (2010)). Most of the higher-order finite-difference schemes suffer from the upwind source singularity. Special treatments like initializing the traveltime filed in a fixed grid-independent region of constant velocity near the source point are employed in order to obtain high accuracy (e.g. Sethian (1999); Zhang et al. (2006); Serna and Qian (2010); Benamou et al. (2010)). These methods have drawbacks such as: (1) the velocity may not be homogeneous near the source, and/or (2) the size of the region of analytic computations must be set by the user and bears no direct relation to the grid parameters. The drawbacks of these methods can be overcome with the adaptive grid refinement method as proposed in Qian and Symes (2002a). However, the adaptive grid refinement method incurs a heavy burden in numerical implementations.

In Luo and Qian (2010), these difficulties are overcome with a factorization approach. Inspired by the factored eikonal equation in Fomel et al. (2009), the authors proposed to factor the takeoff angle additively and the out-of-plane curvature multiplicatively so that the source singularities are well-captured by known functions corresponding to constant velocities. Then a weighted essentially non-oscillatory (WENO) (Liu et al. (1994); Jiang and Shu (1996); Jiang and Peng (2000)) based

Lax-Friedrichs scheme was designed to compute the resulting underlying functions which are smooth near the source point. Thus, the traveltime, the takeoff angle and the amplitude can be obtained with high accuracy. In this companion work, we apply this factorization approach directly to the amplitude without calculating the takeoff angle and the out-of-plane curvature. We factor the amplitude into two multiplicative factors, one of which is the amplitude for homogeneous media. This factor captures the source singularity so that the other factor (the underlying function) is smooth near the source. Then we apply the third-order WENO based Lax-Friedrichs sweeping scheme (Luo and Qian (2010); Kao et al. (2004); Zhang et al. (2006)) to numerically compute the underlying function. Therefore, we can compute the amplitude accurately in both 2-D and 3-D cases.

The paper is organized as follows. We start to present the methodology by first recalling the factorization for the traveltime in Fomel et al. (2009) and Luo and Qian (2010), then we present the factorization for the amplitude. We further present the third-order WENO based Lax-Friedrichs scheme to solve the factored equations in 3-D (Luo and Qian (2010); Kao et al. (2004); Zhang et al. (2006)). Both 2-D and 3-D numerical examples are presented in the numerical experiments. We use our results to construct the asymptotic Green functions and compare the resulting Green functions with those obtained by the Helmholtz solver in Erlangga et al. (2006) and Engquist and Ying (2010). Some remarks are given at the end.

METHODOLOGY

Traveltime and amplitude

For a source (x_0, y_0, z_0) in an isotropic solid, the traveltime $\tau(x, y, z)$ is the viscosity solution of an eikonal equation (Lions (1982); Crandall and Lions (1983)),

$$|\nabla\tau| = s(x, y, z), \tag{1}$$

with the initial condition,

$$\lim_{(x,y,z)\to(x_0,y_0,z_0)} \left(\frac{\tau(x,y,z)}{\sqrt{(x-x_0)^2+(y-y_0)^2+(z-z_0)^2}} - \frac{1}{v(x,y,z)} \right) = 0, \tag{2}$$

where $v = 1/s$ is the velocity.

Based on the traveltime field, one can approximate the amplitude field by solving a transport equation (Cerveny et al. (1977)),

$$\nabla\tau \cdot \nabla A + \frac{1}{2} A \nabla^2 \tau = 0. \tag{3}$$

Equation (3) is a first-order advection equation for the amplitude A. In order to get a first-order accurate amplitude field, one needs a third-order accurate traveltime field since the Laplacian of the traveltime field is involved (Qian and Symes (2002a); Symes (1995)).

The traveltime τ and the amplitude A have an upwind singularity at the source (x_0, y_0, z_0). Any first-order or higher-order finite-difference eikonal solvers or finite-difference methods for the amplitude can formally have at most first-order convergence and large errors, because the low accuracy near the source can spread out to the whole space. In Qian and Symes (2002a), an adaptive method based on the WENO technique for the paraxial eikonal equation overcomes this difficulty. The mesh needs to be refined near the source until expected accuracy requirement is satisfied. In Fomel et al. (2009), the traveltime is factorized into two multiplicative factors, one of which is already known and captures the source singularity. This factorization results in an underlying function that is smooth in a neighborhood of the source. The underlying function satisfies a factored eikonal equation. Numerical schemes can be designed to compute the underlying function. As a consequence, the accuracy of the traveltime can be greatly improved as demonstrated in Fomel et al. (2009). This factorization approach has been extended in Luo and Qian (2010) for takeoff angles and out-of-plane curvatures to obtain reliable amplitudes. Takeoff angles can be decomposed into two additive factors and out-of-plane curvatures can be decomposed into two multiplicative factors.

In both cases, one of the two factors is known corresponding to homogeneous media and captures the source singularity.

In this work, as a companion paper to a previous work (Luo and Qian (2010)), we apply the factorization idea to the amplitude A in the transport equation (3). We decompose A into two multiplicative factors. One of them is the amplitude corresponding to a constant velocity field, and it is known analytically. The factorization of A results in an underlying function that satisfies a factored advection equation. For the factored equations, we use the Lax-Friedrichs scheme based on third-order WENO differences (Luo and Qian (2010); Kao et al. (2004); Zhang et al. (2006)) to solve them numerically.

Factorization of traveltime and amplitude

Let us consider the following factored decompositions (Fomel et al. (2009); Luo and Qian (2010)),

$$\begin{cases} \tau(x,y,z) = \tau_0(x,y,z)u(x,y,z), \\ s(x,y,z) = s_0(x,y,z)\alpha(x,y,z), \end{cases} \tag{4}$$

and assume that τ_0 satisfies

$$|\nabla \tau_0| = s_0, \tag{5}$$

with the initial condition,

$$\lim_{(x,y,z)\to(x_0,y_0,z_0)} \left(\frac{\tau_0(x,y,z)}{\sqrt{(x-x_0)^2+(y-y_0)^2+(z-z_0)^2}} - s_0(x,y,z) \right) = 0. \tag{6}$$

If we choose s_0 as some constant, we have

$$\tau_0 = \frac{\sqrt{(x-x_0)^2+(y-y_0)^2+(z-z_0)^2}}{v_0},$$

which is the traveltime corresponding to the constant velocity field $v_0 = 1/s_0$.

The function substitution transforms the eikonal equation (1) into the factored eikonal equation (Fomel et al. (2009); Luo and Qian (2010)),

$$\sqrt{\tau_0^2|\nabla u|^2 + 2\tau_0 u \nabla\tau_0 \cdot \nabla u + u^2 s_0^2} = s. \tag{7}$$

The factor τ_0 captures the source singularity such that the underlying function u is smooth in a neighborhood of the source.

Denote A_0 as the amplitude corresponding to the constant velocity v_0, and consider the following decomposition for A,

$$A(x, y, z) = A_0(x, y, z)D(x, y, z). \tag{8}$$

Substituting $A = A_0 D$ and $\tau = \tau_0 u$ into (3), we get the factored transport equation,

$$A_0(\tau_0\nabla u + u\nabla\tau_0) \cdot \nabla D + (\tau_0\nabla u \cdot \nabla A_0 + A_0\nabla\tau_0 \cdot \nabla u + \frac{1}{2}A_0\tau_0\Delta u)D = 0. \tag{9}$$

A_0 is known analytically and captures the source singularity, thus the underlying factor D is smooth in a neighborhood of the source.

In order to get first-order accurate A, we need first-order accurate D. In the factored transport equation (9), in order to get first-order accurate D, we need at least third-order accurate u, since Δu is involved. Therefore we need to solve the factored eikonal equation (7) for u with at least third-order accuracy. The traveltime τ_0 and the amplitude A_0 corresponding to the constant velocity field v_0 capture the source singularity properly, which makes it easy to design high order methods to solve (7) and (9) for the underlying functions u and D.

Lax-Friedrichs scheme based on third-order WENO

We present the Lax-Friedrichs scheme for the factored equations (7) and (9) on a rectangular mesh Ω^h with grid size h covering the domain Ω (Luo and Qian (2010); Kao et al. (2004); Zhang et al. (2006)). Let us consider equations in the following general form,

$$H(x, y, z, u, u_x, u_y, u_z) = f(x, y, z). \tag{10}$$

At grid point $(i, k, j) = (x_i, y_k, z_j)$ with neighbors,

$$\begin{aligned} N\{i,k,j\} = &\{(x_{i-1}, y_k, z_j), (x_{i+1}, y_k, z_j), (x_i, y_k, z_{j-1}), \\ &(x_i, y_k, z_{j+1}), (x_i, y_{k+1}, z_j), (x_i, y_{k-1}, z_j)\}, \end{aligned}$$

we consider a Lax-Friedrichs Hamiltonian (Osher and Shu (1991); Kao et al. (2004); Luo and Qian (2010)),

$$\begin{aligned} &H^{LF}(x_i, y_k, z_j, u_{i,k,j}, u_{N\{i,k,j\}}) \\ &= H\left(x_i, y_k, z_j, u_{i,k,j}, \frac{u_{i+1,k,j} - u_{i-1,k,j}}{2h}, \frac{u_{i,k+1,j} - u_{i,k-1,j}}{2h}, \frac{u_{i,k,j+1} - u_{i,k,j-1}}{2h}\right) \\ &- \alpha_x \frac{u_{i+1,k,j} - 2u_{i,k,j} + u_{i-1,k,j}}{2h} - \alpha_y \frac{u_{i,k+1,j} - 2u_{i,k,j} + u_{i,k-1,j}}{2h} \\ &- \alpha_z \frac{u_{i,k,j+1} - 2u_{i,k,j} + u_{i,k,j-1}}{2h}, \end{aligned} \tag{11}$$

where α_x, α_y and α_z are chosen such that for fixed (x_i, y_k, z_j),

$$\begin{aligned} &\frac{\partial H^{LF}}{\partial u_{i,k,j}} \geq 0, \\ &\frac{\partial H^{LF}}{\partial u_{N\{i,k,j\}}} \leq 0. \end{aligned} \tag{12}$$

For example, we can choose,

$$\begin{aligned}
\alpha_x &= \max_{m\le u\le M, A\le p\le B, C\le q\le D, E\le r\le F} \left\{ \frac{1}{2}|H_1(x,y,z,u,p,q,r)| + |\frac{\partial H}{\partial u}(x,y,z,u,p,q,r)| \right\}, \\
\alpha_y &= \max_{m\le u\le M, A\le p\le B, C\le q\le D, E\le r\le F} \left\{ \frac{1}{2}|H_2(x,y,z,u,p,q,r)| + |\frac{\partial H}{\partial u}(x,y,z,u,p,q,r)| \right\}, \\
\alpha_z &= \max_{m\le u\le M, A\le p\le B, C\le q\le D, E\le r\le F} \left\{ \frac{1}{2}|H_3(x,y,z,u,p,q,r)| + |\frac{\partial H}{\partial u}(x,y,z,u,p,q,r)| \right\},
\end{aligned} \tag{13}$$

where H_1, H_2 and H_3 denote the derivatives of H with respect to the first, second and third gradient variable, respectively. The flux H^{LF} is monotone for $m \le u_{i,k,j} \le M, A \le p \le B$, $C \le q \le D$ and $E \le r \le F$ with $p = (u_{i+1,k,j} - u_{i-1,k,j})/2h$, $q = (u_{i,k+1,j} - u_{i,k-1,j})/2h$ and $r = (u_{i,k,j+1} - u_{i,k,j-1})/2h$. Then we have a first-order Lax-Friedrichs scheme,

$$\begin{aligned}
&u_{i,k,j}^{new} = \\
&\left(\frac{1}{\alpha_x/h + \alpha_y/h + \alpha_z/h}\right) \times \\
&\left[f_{i,k,j} - H\left(x_i, y_k, z_j, u_{i,k,j}^{old}, \frac{u_{i+1,k,j} - u_{i-1,k,j}}{2h}, \frac{u_{i,k+1,j} - u_{i,k-1,j}}{2h}, \frac{u_{i,k,j+1} - u_{i,k,j-1}}{2h}\right) \right. \\
&\left. + \alpha_x \frac{u_{i+1,k,j} + u_{i-1,k,j}}{2h} + \alpha_y \frac{u_{i,k+1,j} + u_{i,k-1,j}}{2h} + \alpha_z \frac{u_{i,k,j+1} + u_{i,k,j-1}}{2h} \right].
\end{aligned} \tag{14}$$

As in Zhang et al. (2006) and Luo and Qian (2010), we replace $u_{i-1,k,j}$, $u_{i+1,k,j}$, $u_{i,k+1,j}$, $u_{i,k-1,j}$, $u_{i,k,j-1}$ and $u_{i,k,j+1}$ with,

$$\begin{aligned}
u_{i-1,k,j} &= u_{i,k,j} - h(u_x)^-_{i,k,j}, \ u_{i+1,k,j} = u_{i,k,j} + h(u_x)^+_{i,k,j}; \\
u_{i,k-1,j} &= u_{i,k,j} - h(u_y)^-_{i,k,j}, \ u_{i,k+1,j} = u_{i,k,j} + h(u_y)^+_{i,k,j}; \\
u_{i,k,j-1} &= u_{i,k,j} - h(u_z)^-_{i,k,j}, \ u_{i,k,j+1} = u_{i,k,j} + h(u_z)^+_{i,k,j}.
\end{aligned} \tag{15}$$

$(u_x)^-_{i,k,j}$ and $(u_x)^+_{i,k,j}$ are third-order WENO approximations of u_x, $(u_y)^-_{i,k,j}$ and $(u_y)^+_{i,k,j}$ are third-order WENO approximations of u_y, and $(u_z)^-_{i,k,j}$ and $(u_z)^+_{i,k,j}$ are third-order WENO approximations of u_z; see Osher and Shu (1991), Liu et al. (1994), Jiang and Shu (1996) and Jiang and Peng

(2000). For example,

$$(u_x)^-_{i,k,j} = (1-\omega_-)\left(\frac{u_{i+1,k,j}-u_{i-1,k,j}}{2h}\right) + \omega_-\left(\frac{3u_{i,k,j}-4u_{i-1,k,j}+u_{i-2,k,j}}{2h}\right) \tag{16}$$

with

$$\omega_- = \frac{1}{1+2\gamma_-^2},\ \gamma_- = \frac{\epsilon+(u_{i,k,j}-2u_{i-1,k,j}+u_{i-2,k,j})^2}{\epsilon+(u_{i+1,k,j}-2u_{i,k,j}+u_{i-1,k,j})^2}, \tag{17}$$

and

$$(u_x)^+_{i,k,j} = (1-\omega_+)\left(\frac{u_{i+1,k,j}-u_{i-1,k,j}}{2h}\right) + \omega_+\left(\frac{-3u_{i,k,j}+4u_{i+1,k,j}-u_{i+2,k,j}}{2h}\right) \tag{18}$$

with

$$\omega_+ = \frac{1}{1+2\gamma_+^2},\ \gamma_+ = \frac{\epsilon+(u_{i,k,j}-2u_{i+1,k,j}+u_{i+2,k,j})^2}{\epsilon+(u_{i+1,k,j}-2u_{i,k,j}+u_{i-1,k,j})^2}. \tag{19}$$

Similarly, we can define third-order WENO approximations for $(u_y)^-_{i,k,j}$, $(u_y)^+_{i,k,j}$, $(u_z)^-_{i,k,j}$ and $(u_z)^+_{i,k,j}$. ϵ is a small positive number to avoid division by zero.

Then we have a Lax-Friedrichs scheme based on the third-order WENO approximations (Zhang et al. (2006); Luo and Qian (2010)),

$$\begin{aligned}
&u^{new}_{i,k,j} = \\
&\left(\frac{1}{\alpha_x/h+\alpha_y/h+\alpha_z/h}\right)\times \\
&\left[f_{i,k,j} - H\left(x_i, y_k, z_j, u^{old}_{i,k,j}, \frac{(u_x)^-_{i,k,j}+(u_x)^+_{i,k,j}}{2}, \frac{(u_y)^-_{i,k,j}+(u_y)^+_{i,k,j}}{2}, \frac{(u_z)^-_{i,k,j}+(u_z)^+_{i,k,j}}{2}\right)\right. \\
&+\alpha_x\frac{2u^{old}_{i,k,j}+h((u_x)^+_{i,k,j}-(u_x)^-_{i,k,j})}{2h} + \alpha_y\frac{2u^{old}_{i,k,j}+h((u_y)^+_{i,k,j}-(u_y)^-_{i,k,j})}{2h} \\
&\left.+\alpha_z\frac{2u^{old}_{i,k,j}+h((u_z)^+_{i,k,j}-(u_z)^-_{i,k,j})}{2h}\right].
\end{aligned} \tag{20}$$

$u^{new}_{i,k,j}$ denotes the to-be-updated numerical solution for u at the grid point (i,k,j) and $u^{old}_{i,k,j}$ denotes the current old value for u at the same point.

The third-order Lax-Friedrichs sweeping method for equation (10) is summarized as follows

(Kao et al. (2004); Zhang et al. (2006); Luo and Qian (2010)):

1 Initialization: assign exact values or interpolate values at grid points within a cubic volume centered at the source point with side equal to $2h + 2h$, such that the grid points are enough for the third-order WENO approximations. These values are fixed during iterations.

2 Iterations: update $u_{i,k,j}^{new}$ in (20) by Gauss-Seidel iterations with eight alternating directions:

$$(1)\ i = 1 : I, k = 1 : K, j = 1 : J;\ \ (2)\ i = 1 : I, k = 1 : K, j = J : 1;$$

$$(3)\ i = 1 : I, k = K : 1, j = 1 : J;\ \ (4)\ i = 1 : I, k = K : 1, j = J : 1;$$

$$(5)\ i = I : 1, k = 1 : K, j = 1 : J;\ \ (6)\ i = I : 1, k = 1 : K, j = J : 1;$$

$$(7)\ i = I : 1, k = K : 1, j = 1 : J;\ \ (8)\ i = I : 1, k = K : 1, j = J : 1.$$

3 Convergence: if

$$|u_{i,k,j}^{new} - u_{i,k,j}^{old}|_\infty \leq \delta,$$

where δ is a given convergence threshold value, the iterations converge and stop.

We use this scheme to solve the factored equations:

- **Equation (7)** with Hamiltonian and f as,

$$H(x, y, z, u, u_x, u_y, u_z) = \sqrt{\tau_0^2|\nabla u|^2 + 2\tau_0 u \nabla\tau_0 \cdot \nabla u + u^2 s_0^2},$$

$$f = s.$$

- **Equation (9)** with Hamiltonian and f as,

$$\begin{aligned}&H(x,y,z,D,D_x,D_y,D_z) = \\ &A_0(\tau_0\nabla u + u\nabla\tau_0)\cdot\nabla D + (\tau_0\nabla u\cdot\nabla A_0 + A_0\nabla\tau_0\cdot\nabla u + \frac{1}{2}A_0\tau_0\Delta u)D, \\ &f = 0.\end{aligned}$$

NUMERICAL EXPERIMENTS

In this section, we present several 2-D and 3-D examples to demonstrate the performance of the method.

2-D Examples

For all 2-D examples, we show results computed with our method, and we use computed results to approximate the Green functions for the Helmholtz equation with high frequencies,

$$\nabla^2 G_2(x,y,\omega) + \frac{\omega^2}{v^2(x,y)}G_2(x,y,\omega) = -\delta(x-x_0)\delta(y-y_0), \tag{21}$$

where $G_2(x,y,\omega)$ is the Green function dependent on the frequency ω.

We approximate the 2-D Green function in the WKBJ form (Appendix C in Leung et al. (2007)),

$$G_2(x,y,\omega) \approx \frac{1}{\sqrt{\omega}}A(x,y)e^{i(\omega\tau(x,y)+\frac{\pi}{4})}. \tag{22}$$

First we use the following two velocity models, and we compare our results with the solutions computed with a Helmholtz solver (Erlangga et al. (2006)). We choose $\omega = 32\pi$.

1. Constant velocity $v(x,y) \equiv 5.0$, $(x_0,y_0) = (0.5, 0.5)$, and domain $[0,\ 1]\times[0,\ 1]$. We apply our method on a 100×100 mesh and solve the Helmholtz equation (21) with the Helmholtz solver (Erlangga et al. (2006)) on a 1200×1200 mesh. Figure 1 shows the traveltime and

amplitude computed with our method. Figure 2 shows the results for the 2-D Green function on a 100 × 100 mesh. The results by our method are very close to those obtained by the Helmholtz solver. The reason is that the traveltime field is smooth everywhere away from the source. Therefore, the constructed asymptotic Green function approximates the true Green function faithfully.

2. Velocity $v(x, y) = 1+0.2 \sin(0.5\pi y) \sin(3\pi(x+0.05))$, $(x_0, y_0) = (0.5, 0.1)$, and domain $[0,\ 1] \times [0,\ 2]$. We apply our method on a 200 × 100 mesh and solve the Helmholtz equation (21) with the Helmholtz solver in Erlangga et al. (2006) on a 1600 × 800 mesh. Figure 3 shows the velocity model and the resulting traveltime and amplitude computed by our method. Figure 4 shows the results for the 2-D Green function on a 200 × 100 mesh; especially we plot two slices at $y = 0.3$ (no kink, no caustics) and at $y = 1.5$ (kink, caustics). The constructed Green function in the weak sense can not approximate the true Green function faithfully because the traveltime field is not smooth. However, we notice that before the kinks appear in the single-valued traveltime field or caustics appear in the multi-valued traveltime field, the true traveltime filed is smooth and the asymptotic Green function in the single-valued sense approximate the true Green function faithfully. Only after the kinks in the single-valued traveltime field or caustics in the multi-valued traveltime field appear, the two traveltime fields yield totally different Green functions.

Marmousi velocity model

We consider the smooth Marmousi velocity model as in Figure 5. Note that the velocity is rescaled by a factor 10^{-4}. The traveltime and amplitude computed with our method are shown in Figure 5. Figure 6 shows the constructed Green function with $\omega = 32\pi$.

In this model, we see kinks in the computed traveltime field and discontinuities in the computed amplitude and constructed WKBJ Green function.

3-D Examples

We use three 3-D velocity models to demonstrate the performance of our method. With the computed amplitude, we approximate the 3-D Green functions for the Helmholtz equation with high frequencies,

$$\nabla^2 G_3(x,y,z,\omega) + \frac{\omega^2}{v^2(x,y,z)} G_3(x,y,z,\omega) = -\delta(x-x_0)\delta(y-y_0)\delta(z-z_0), \tag{23}$$

where $G_3(x,y,z,\omega)$ is the Green function dependent on the frequency ω.

We approximate the 3-D Green function in the WKBJ form (Appendix C in Leung et al. (2007)),

$$G_3(x,y,z,\omega) \approx A(x,y,z) e^{i\omega\tau(x,y,z)}. \tag{24}$$

3-D example 1: constant velocity. The velocity $v \equiv 5$. The domain is $[-1,\ 1] \times [-1,\ 1] \times [-1,\ 2]$. We use an $81 \times 81 \times 121$ mesh. The source point is at $(x_0, y_0, z_0) = (0,0,0)$. We choose $\omega = 64\pi$. Figure 7 shows the computed traveltime, amplitude and constructed Green functions. In Figure 8, we compare our computed amplitude with the exact amplitude,

$$A(x,y,z) = \frac{1}{4\pi\sqrt{(x-x_0)^2 + (y-y_0)^2 + (z-z_0)^2}},$$

at $(y = 0, z = 0.3)$ and $(y = 0, z = 1.5)$. In Figure 9, we compare the constructed Green functions with the exact asymptotic form obtained in Leung et al. (2007) at $(y = 0, z = 0.3)$ and $(y = 0, z = 1.5)$. The computed amplitude and constructed Green function are very accurate.

3-D example 2: Vinje's Gaussian model. The velocity model is given by,

$$v(x,y,z) = 4 - 1.75 e^{-\frac{((2x-1)^2 + (2y-1)^2 + (2z-1.75)^2)}{0.5^2}}. \tag{25}$$

The domain is $[0,\ 1] \times [0,\ 1] \times [0,\ 1]$. The velocity field v is rescaled by a factor $2/(\max_{0 \le x,y,z \le 1} v +$

$\min_{0\leq x,y,z\leq 1} v)$. We use a $159 \times 159 \times 159$ mesh. The source point is at $(x_0, y_0, z_0) = (0.5, 0.5, 0.5)$. We choose $\omega = 40\pi$. Figure 10 shows the computed traveltime, amplitude and constructed Green functions at $z = 29/158$ and $z = 109/158$.

Figure 11 shows the comparisons between constructed WKBJ Green function and that obtained by the Helmholtz solver in Engquist and Ying (2010) at $z = 29/158$ and $z = 109/158$. In Figure 12, we show comparisons at $(y = 79/158, z = 29/158)$ and $(y = 79/158, z = 109/158)$. The constructed Green functions are very accurate.

3-D example 3: waveguide model. The velocity model is given by,

$$v(x, y, z) = 1.5 - e^{-0.5(2x-1)^2}. \tag{26}$$

The domain is $[0,\ 1]\times[0,\ 1]\times[0,\ 1]$. The velocity field v is rescaled by a factor $2/(\max_{0\leq x,y,z\leq 1} v + \min_{0\leq x,y,z\leq 1} v)$. We use a $159 \times 159 \times 159$ mesh. The source point is at $(x_0, y_0, z_0) = (0.5, 0.5, 0.5)$. We choose $\omega = 40\pi$. Figure 13 shows the computed traveltime, amplitude and constructed Green functions at $z = 29/158$ and $z = 109/158$. Figure 14 shows more wavefields of constructed Green functions with our method.

CONCLUSIONS

As a companion work to Luo and Qian (2010), we apply the factorization technique based on the factored eikonal equation (Fomel et al. (2009); Luo and Qian (2010)) directly to compute the amplitude. We decompose the amplitude into two multiplicative factors. One of them is known analytically corresponding to a constant velocity field, and it captures the source singularity of the amplitude. Then we apply the third-order WENO based Lax-Friedrichs sweeping method (Kao et al. (2004); Zhang et al. (2006); Luo and Qian (2010)) to solve the factored equations for the underlying function numerically. The advantage of decomposing the amplitude into tow multiplicative factors is that since the known factor captures the source singularity, the other factor is smooth at the source. With computed traveltime and amplitude, we construct the asymptotic Green functions in both 2-D and 3-D cases. Numerical examples are presented to demonstrate the performance of our method.

ACKNOWLEDGMENT

Qian is partially supported by NSF 0810104 and NSF 0830161. Zhao is partially supported by DMS-0811254.

REFERENCES

Benamou, J. D., Luo, S., and Zhao, H.-K., 2010, A Compact Upwind Second Order Scheme for the Eikonal Equation: J. Comp. Math., **28**, 489–516.

Cerveny, V., Molotkov, I. A., and Psencik, I., 1977, Ray method in seismology: Univ. Karlova Press.

Crandall, M. G., and Lions, P.-L., 1983, Viscosity solutions of Hamilton-Jacobi equations: Tans. Amer. Math. Soc., **277**, 1–42.

Engquist, B., and Ying, L., 2010, Sweeping preconditioner for the Helmholtz equation: Moving perfectly matched layers: preprint.

Erlangga, Y. A., Oosterlee, C. W., and Vuik, C., 2006, A novel multigrid-based preconditioner for the heterogeneous Helmholtz equation: SIAM Journal on Scientific Computing, **27**, 1471–1492.

Fomel, S., Luo, S., and Zhao, H.-K., 2009, Fast sweeping method for the factored eikonal equation: Journal of Comp. Phys., **228**, no. 17, 6440–6455.

Jiang, G. S., and Peng, D., 2000, Weighted ENO schemes for Hamilton-Jacobi equations: SIAM J. Sci. Comput., **21**, 2126–2143.

Jiang, G. S., and Shu, C. W., 1996, Efficient implementation of weighted ENO schemes: J. Comput. Phys., **126**, 202–228.

Kao, C. Y., Osher, S., and Qian, J., 2004, Lax-Friedrichs sweeping schemes for static Hamilton-Jacobi equations: Journal of Computational Physics, **196**, 367–391.

Kao, C. Y., Osher, S., and Tsai, Y., 2005, Fast sweeping method for static Hamilton-Jacobi equations: SIAM Journal on Numerical Analysis, **42**, 2612–2632.

Kim, S., and Cook, R., 1999, 3-D traveltime computation using second-order ENO scheme: Geophysics, **64**, 1867–1876.

Leung, S., and Qian, J., 2006, An adjoint state method for three-dimensional transmission traveltime tomography using first-arrivials: Comm. Math. Sci., **4**, no. 1, 249–266.

Leung, S., Qian, J., and Burridge, R., 2007, Eulerian Gaussian beams for high-frequency wave propagation: Geophysics, **72**, no. 5, SM61–SM76.

Lions, P.-L., 1982, Generalized solutions of Hamilton-Jacobi equations: Pitman, Boston.

Liu, X. D., Osher, S. J., and Chan, T., 1994, Weighted Essentially NonOscillatory schemes: J. Comput. Phys., **115**, 200–212.

Luo, S., and Qian, J., 2010, Factored singularities and high-order Lax-Friedrichs sweeping schemes for point-source traveltimes and amplitudes: submitted.

Osher, S., and Shu, C.-W., 1991, High-order essentially nonoscillatory schemes for Hamilton-Jacobi equations: SIAM J. Math. Anal., **28**, no. 4, 907–922.

Qian, J., and Symes, W. W., 2002a, An Adaptive Finite-Difference Method for Traveltimes and Amplitudes: Geophysics, **67**, 167–176.

——— 2002b, Finite-difference quasi-P traveltimes for anisotropic media: Geophysics, **67**, 147–155.

Qian, J., Zhang, Y.-T., and Zhao, H.-K., 2007a, A fast sweeping methods for static convex Hamitlon-Jacobi equations: Journal of Scientific Computings, **31(1/2)**, 237–271.

——— 2007b, Fast sweeping methods for eiknonal equations on triangulated meshes: SIAM J. Numer. Anal., **45**, 83–107.

Qin, F., Luo, Y., Olsen, K. B., Cai, W., and Schuster, G. T., 1992, Finite difference solution of the eikonal equation along expanding wavefronts: Geophysics, **57**, 478–487.

Schneider, W. A. J., Ranzinger, K., Balch, A., and Kruse, C., 1992, A dynamic programming approach to first arrival traveltime computation in media with arbitrarily distributed velocities: Geophysics, **57**, 39–50.

Schneider, W. A. J., 1995, Robust and efficient upwind finite-difference traveltime calculations in three dimensions: Geophysics, **60**, 1108–1117.

Serna, S., and Qian, J., 2010, A stopping criterion for higher-order sweeping schemes for static Hamilton-Jacobi equations: J. Comp. Math., **28**, 552–568.

Sethian, J. A., and Popovici, A. M., 1999, 3-D traveltime computation using the fast marching method: Geophysics, **64**, no. 2, 516–523.

Sethian, J. A., 1999, Level Set Methods and Fast Marching Methods: Evolving Interfaces in Computational Geometry, Fluid Mechanics, Computer Vision, and Materials Science: Cambridge University Press.

Symes, W. W., 1995, Mathematics of reflection seismology: Annual Report: The Rice Invesion Project (http://www.trip.caam.rice.edu).

Tsai, Y.-H. R., Cheng, L.-T., Osher, S., and Zhao, H.-K., 2003, Fast sweeping algorithms for a class of Hamilton-Jacobi equations: SIAM Journal on Numerical Analysis, **41**, 673–694.

van Trier, J., and Symes, W. W., 1991, Upwind finite-difference calculation of traveltimes: Geophysics, **56**, no. 6, 812–821.

Vidale, J. E., 1990, Finite-difference calculation of traveltimes in three dimensions: Geophysics, **55**, no. 05, 521–526.

Zhang, Y.-T., Zhao, H.-K., and Qian, J., 2006, High order fast sweeping methods for static Hamilton-Jacobi equations: Journal of Scientific Computing, **29**, 25–56.

Zhao, H.-K., 2005, A fast sweeping method for eikonal equations: Mathematics of Computation, **74**, 603–627.

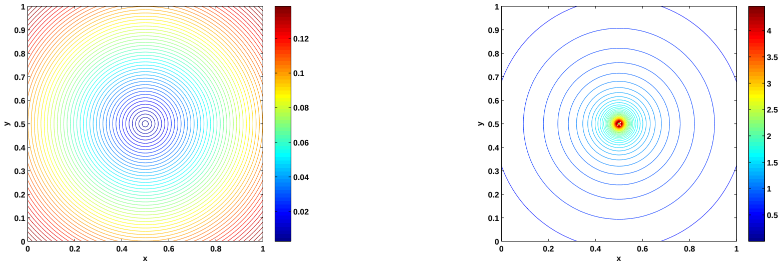

Figure 1: 2-D example case 1. Left: traveltime field; Right: amplitude.

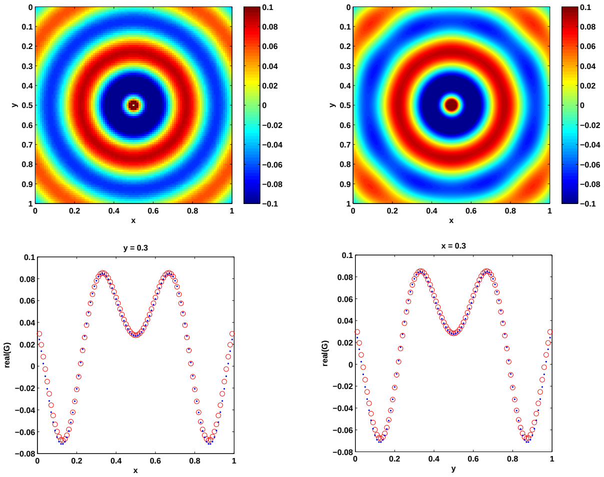

Figure 2: 2-D example case 1. Two-dimensional Green function. Top: image of the real part of the Green function (left: our method, right: Helmholtz solver). Bottom: two slices of the Green function (real part) at $y = 0.3$ (left) and $x = 0.3$ (right). Red circle: our method. Blue dot: Helmholtz solver.

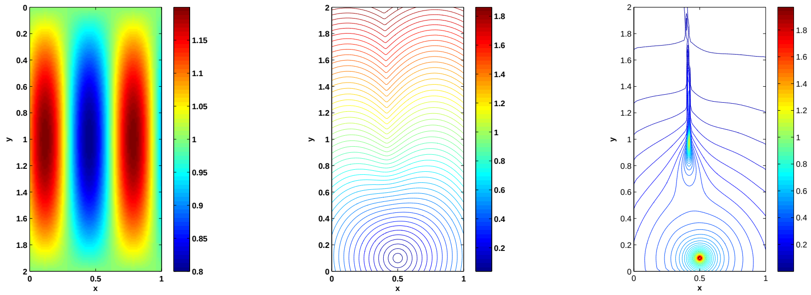

Figure 3: 2-D example case 2. Left: velocity field; Middle: traveltime field; Right: amplitude.

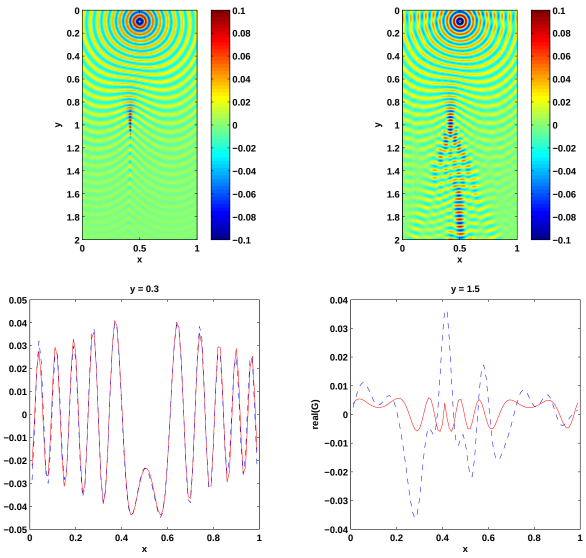

Figure 4: 2-D example case 2. Two-dimensional Green function. Top: image of the real part of the Green function (left: our method, right: Helmholtz solver). Bottom: two slices of the Green function (real part) at $y = 0.3$ (left) and $y = 1.5$ (right). Red line: our method. Blue dash line: Helmholtz solver.

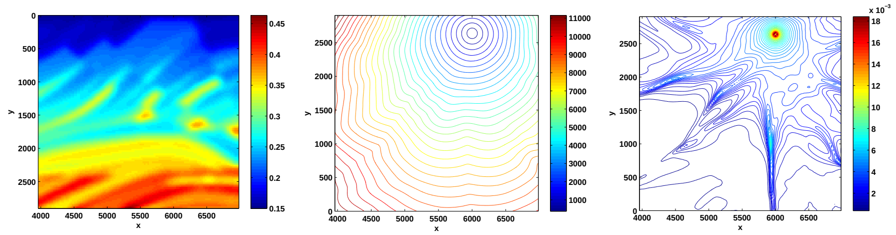

Figure 5: 2-D example with Marmousi velocity model. Left: velocity field; Middle: traveltime; Right: amplitude.

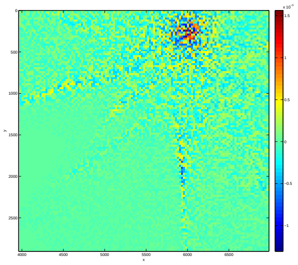

Figure 6: 2-D example with Marmousi velocity model. Constructed Green function with $\omega = 32\pi$.

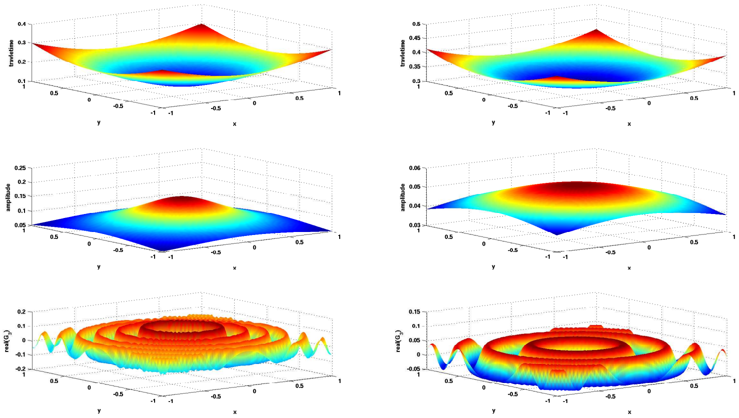

Figure 7: 3-D example 1. From top to bottom: traveltime, amplitude and constructed Green function with $\omega = 64\pi$. Left: $z = 0.3$; Right $z = 1.5$.

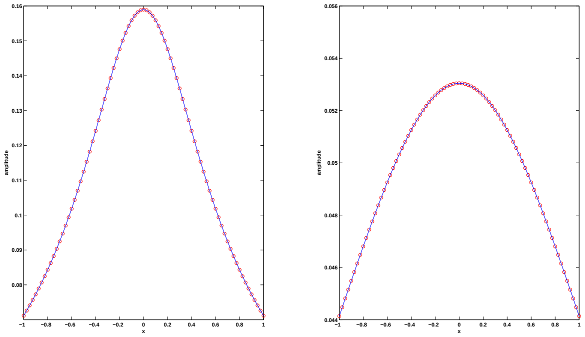

Figure 8: 3-D example 1. Comparison of amplitudes. Left: $(y = 0, z = 0.3)$; Right: $(y = 0, z = 1.5)$. Red circle: our method; Blue line: exact amplitude.

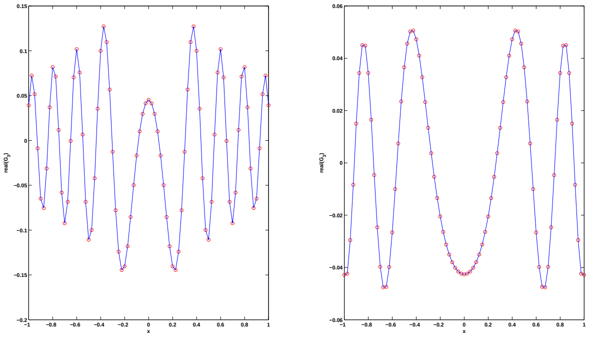

Figure 9: 3-D example 1. Comparison of constructed Green functions. Left: $(y = 0, z = 0.3)$; Right: $(y = 0, z = 1.5)$. Red circle: our method; Blue line: exact asymptotic form.

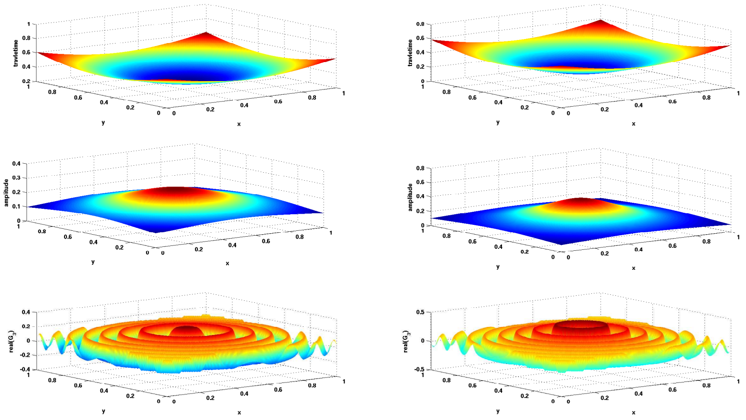

Figure 10: 3-D example 2. From top to bottom: traveltime, amplitude and constructed Green function with $\omega = 40\pi$. Left: $z = 29/158$; Right $z = 109/158$.

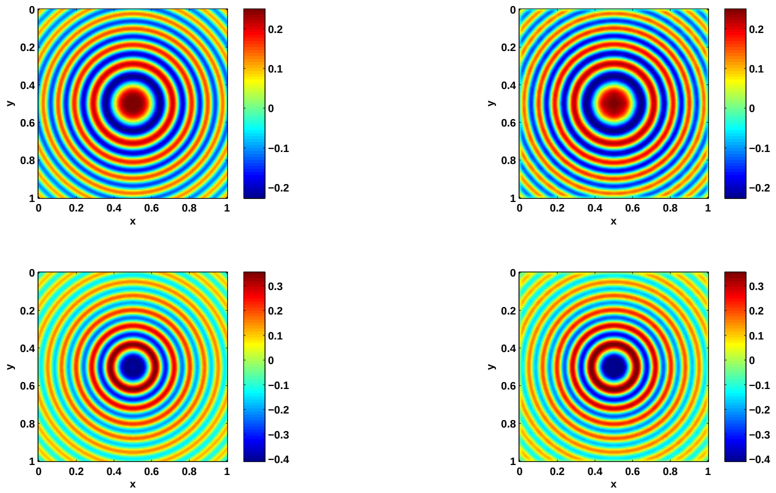

Figure 11: 3-D example 2. Comparison of constructed Green functions. Top: $z = 29/158$; Bottom: $z = 109/158$. Left: our method; Right: Helmholtz solver.

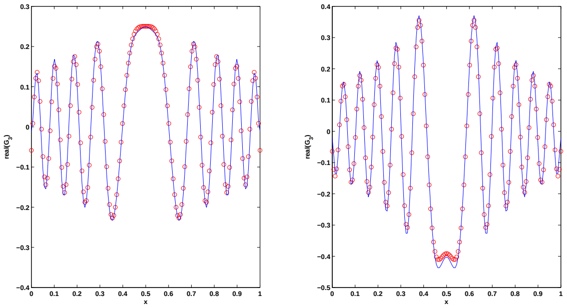

Figure 12: 3-D example 2. Comparison of constructed Green functions. Left: ($y = 79/158, z = 29/158$); Right: ($y = 79/158, z = 109/158$). Red circle: our method; Blue line: Helmholtz solver.

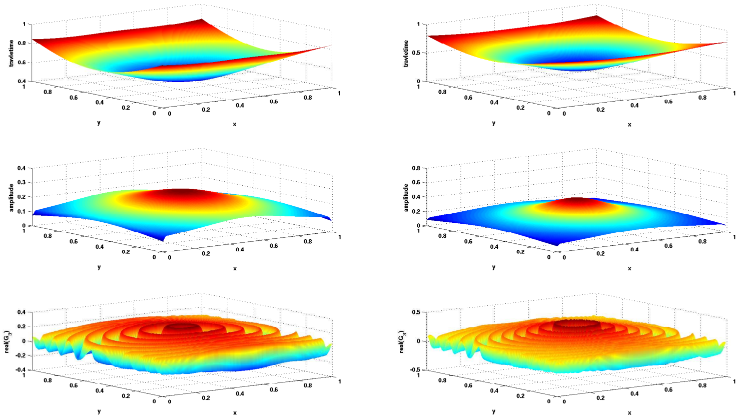

Figure 13: 3-D example 3. From top to bottom: traveltime, amplitude and constructed Green function with $\omega = 40\pi$. Left: $z = 29/158$; Right $z = 109/158$.

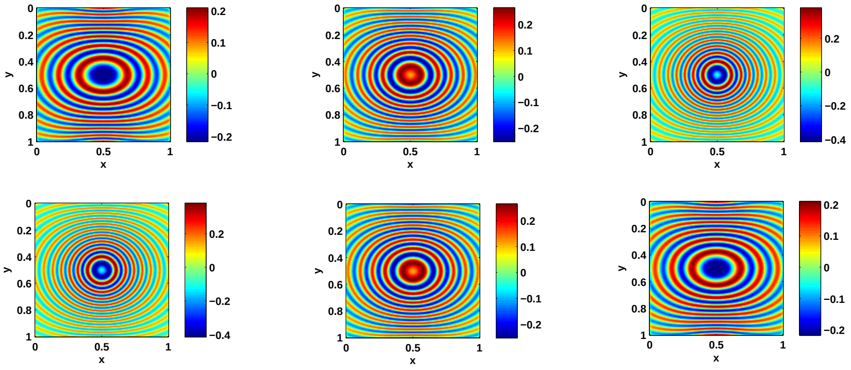

Figure 14: 3-D example 3. Constructed Green function with $\omega = 40\pi$. Top: $z = 14/158,\ 29/158,\ 49/158$; Bottom: $z = 109/158,\ 129/158,\ 144/158$.